Density functional study of narrow cubic MnSe nanowires: Role of MnSe chains

Peiman Amiri,[1] S. Javad Hashemifar,[1,2] and Hadi Akbarzadeh[1,2]
[1]*Department of Physics, Isfahan University of Technology, 84156-83111 Isfahan, Iran*
[2]*Nanotechnology and Advanced Materials Institute, Isfahan University of Technology, 84156-83111 Isfahan, Iran*
(Received 20 November 2010; published 18 April 2011)

First-principles pseudopotential calculations are employed to study the structural stability, electronic, and magnetic properties of bulk, free chain, free (100) and (110) surfaces, and narrow [001] nanowires of MnSe in the rock-salt structure. The bulk computations reveal underestimation of the Mn 3*d* spin exchange splitting within generalized gradient approximation (GGA) and hence necessity of the GGA + *U* scheme for improvement of this parameter toward experimental data. The obtained cohesive energies indicate higher stability of narrow MnSe nanowires with (100) facets and sharp square cross sections. A phenomenological model was applied to measure the energy costs for the creation of the facet and edge MnSe chains in MnSe nanowires. Comparing the electronic band structures and cohesive energies of the pristine and hydrogen-passivated MnSe[001] nanowires justifies efficient surface rehybridizations and, consequently, the absence of surface dangling bonds in various MnSe nanostructures.

DOI: 10.1103/PhysRevB.83.165424 PACS number(s): 73.22.−f, 75.75.−c

I. INTRODUCTION

Magnetic chalcogenides and their alloys, because of their magneto optical and transport properties, have great potential applications in infrared detectors, solar cells, and spintronics devices.[1,2] Mn*Y* (*Y* = S, Se, Te) compounds are the end-point ($x = 1$) materials for the wide-gap II-VI semiconductors doped with magnetic Mn impurities: $X_{1-x}Mn_xY$ (*X* = Zn, Cd, Hg and *Y* = S, Se, Te).[3] Among the 3*d* transition-metal chalcogenides, MnS, MnSe, and MnTe are antiferromagnetic (AFM) compounds with respective Neel temperatures of 152,[4] 124,[5] and 307 K.[2]

The room-temperature stable crystal structure of MnSe is a cubic NaCl-type lattice (α phase), with a type II antiferromagnetism along the [111] direction.[6] By decreasing temperature, a second phase with hexagonal NiAs crystal structure may nucleate at about 190 K. Although the contribution of the NiAs grains to the grown MnSe samples increases with decreasing temperature, it does not exceed 15%–38% of crystal volume.[5] Hence, even at very low temperatures, the cubic NaCl-type MnSe grains have the dominant contribution to MnSe samples.[6] The synthesis of α-MnSe quantum wires (diameter of 3 nm) using mesoporous silica templates was reported by Chen *et al.*[7] In 2004 and 2006, α-MnSe nanospheres and nanorods were synthesized using autoclave solvothermal and hydrothermal reactions.[8,9] In 2006, Chun *et al.* used a morphology-tuned growth method to fabricate various 1D α-MnSe nanostructures, including nanowires (NWs) and nanocables.[10] The MnSe nanowires, with average diameter of 70 nm, were grown with a single-crystalline rock-salt structure in the [001] direction.

In spite of several experimental and theoretical studies on the electronic and magnetic properties of bulk MnSe, to our knowledge, there is no first-principles study on 1D MnSe nanostructures. Hence, we found it useful to employ density functional theory to investigate the physical properties of MnSe nanowires. In the following, we first explain our method of computations. Then, the structural, electronic, and magnetic properties of bulk α-MnSe are discussed in detail, and the requirement of the generalized gradient approximation (GGA) + *U* calculations in this system is justified. Next, the optimized value of *U* is applied to study physical properties as well as the stability of pristine MnSe[001] NWs with (100) and (110) facets. Then the calculated total energies are combined with an appropriate phenomenological model to understand surface effects on the stability of various nanowires. In Sec. V, the effects of surface passivation on MnSe nanowires are examined. The summary of our results is presented in the last section.

II. COMPUTATIONAL APPROACH

Our total energy calculations were performed by using the QUANTUM ESPRESSO/PWSCF package, which is based on the density functional theory, and the ultrasoft pseudopotential technique.[11,12] In this code the valence electronic wave functions are expanded in a plane-wave basis set. The Perdew, Burke, and Ernzerhof formalism of the generalized gradient approximation[13] to the exchange-correlation potential was used in this work. After doing enough convergence tests, an energy cutoff of 35 Ry was chosen for plane-wave expansion. The bulk and nanowire Brillouin zone integrations were performed by using Monkhorst-Pack[14] meshes of $(10 \times 10 \times 10)$ and $(1 \times 1 \times 10)$ *k* points, respectively, along with the Methfessel-Paxton[15] method of smearing with a broadening parameter of 0.02 Ry. All structures have been optimized to achieve the minimum energy by accurate relaxation of the atomic positions down to forces less than 1 mRy/bohr. As the bulk electronic structure of MnSe within GGA is considerably different from the measured data (which will be explained), we performed a more accurate electronic structure calculation by using the GGA + *U* method. The free chains, surfaces, and nanowire structures were simulated by using the supercell approach with a vacuum thickness of about 10 Å.

III. BULK PROPERTIES

As discussed in the introduction, the most stable structure of bulk MnSe is the cubic NaCl-type lattice with a type II antiferromagnetism in the [111] direction (AF111).[6] In order

TABLE I. The equilibrium properties of bulk α-MnSe within GGA and GGA + U (U = 2eV); a (Å) is a lattice constant, B (GPa) is bulk modulus, E_C (mRy/atom) is cohesive energy, gap (eV) is band gap, and μ_{Mn} (μ_B) is the magnetization of a Mn atom.

Method	State	a	B	E_C	Gap	μ_{Mn}
GGA	AF111	5.39	65.7	−314	0.8	4.45
	AF001	5.39	57.8	−300	···	4.61
	FM	5.25	83.7	−292	···	3.78
GGA + U	AF111	5.48	61.6	−289	1.30	4.66
Experiment[a]		5.46	56.9		2.0	4.6

[a]Values for a, B, gap, and μ_{Mn} are from Refs. 8, 16, 17, and 18, respectively.

to determine the equilibrium properties of the systems, we accurately optimized the lattice parameters as well as the internal atomic positions of the cubic MnSe in ferromagnetic (FM) and two antiferromagnetic states along [001] (AF001) and [111] (AF111) crystallographic directions within GGA. The obtained equilibrium properties are listed in Table I.

We observe that AF111 is the most stable state within GGA, while in the AF001 and FM states, α-MnSe has a metallic behavior. The energy band structure and partial density of states (DOS) of valence orbitals of AF111 α-MnSe within GGA are displayed in Fig. 1. An indirect energy gap of 0.8 eV is visible between high symmetry T and X points. The gap is enclosed by the occupied Se p and the empty Mn d states. Although GGA is able to predict the correct semiconductor antiferromagnetic state of cubic MnSe, all physical properties and, particularly, band gap differ considerably from experimental data. We attribute this deficiency of GGA to the highly correlated character of the Mn d electrons. The electronic states of Mn s and Se p orbitals responsible for bonding can be described by using conventional (GGA) band calculations. However, the GGA band method may not describe correctly the highly correlated Mn d electrons. Hence, for better description of the electronic structure and magnetic moments of MnSe, we applied the GGA + U scheme to our calculations to enhance on-site correlation of the d states.

In order to determine the appropriate value of the effective Hubbard parameter U for our GGA + U study, we calculated the equilibrium properties of AF111 α-MnSe at different values of U, ranging from 0 to 5 eV. The obtained results are plotted in Fig. 2. Applying U increases on-site correlation of the Mn d electrons and hence decreases their hybridization with valence Se p electrons and, consequently, weakens the Mn-Se bonding in the system. As a result of that, by increasing the effective U parameter, the lattice parameter and magnetization of Mn are enhanced, while the bulk modulus of the system is reduced (Fig. 2). It is observed that the band gap reaches to 1.30 eV at U = 2eV and then becomes insensitive to the value of U. The reason is that, within GGA, the top of the valence band is mainly constituted of the Se p states, while the Mn d and s states have major contributions to the bottom of conduction band, leading to a gap surrounded by the Mn d and Se p states (Fig. 1). Applying U on the Mn d states repels them from the Fermi level and leaves a gap enclosed by the

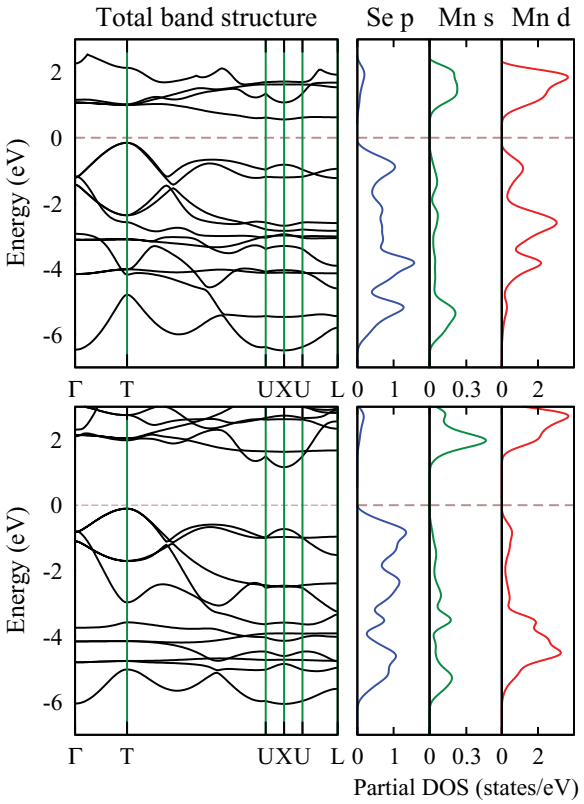

FIG. 1. (Color online) The total band structure and the partial DOS of Se p, Mn s, and Mn d orbitals in AF111 α-MnSe within (top) GGA and (bottom) GGA + U with U = 2 eV. The Fermi energies are set to zero.

Se p and Mn s states, which is reasonably insensitive to the absolute value of the effective U parameter.

The Mn d partial DOS in AF111 α-MnSe at different values of U are sketched in Fig. 3. Sato *et al.*[17] employed the photoemission and inverse-photoemission techniques to study the occupied and unoccupied Mn 3d states in cubic MnSe. They found an exchange splitting of about 7.4 ± 0.2 eV

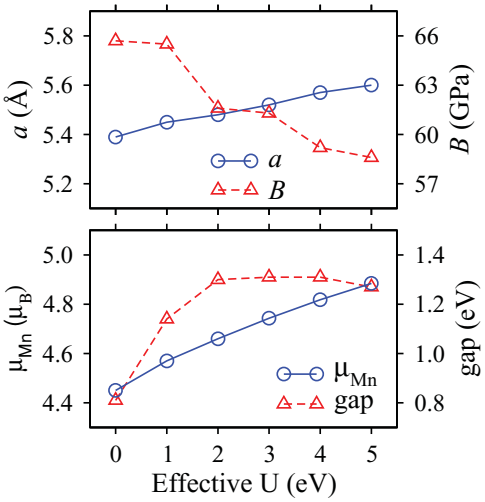

FIG. 2. (Color online) The equilibrium properties of AF111 α-MnSe at different values of U. The parameters have the same meaning as in Table I.

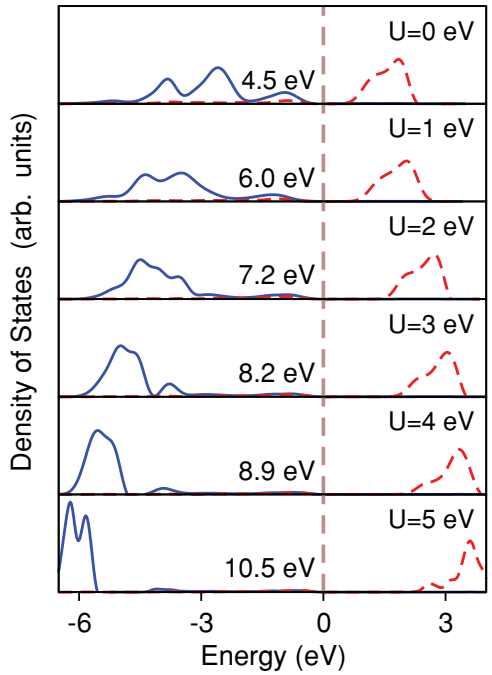

FIG. 3. (Color online) The Mn d partial DOS in AF111 α-MnSe at different values of U. The blue solid and red dashed lines correspond to the majority and minority states. The numbers in the plots are the corresponding Mn d exchange-splitting values. The Fermi energy is set to zero.

and a gap of about 2 eV for the Mn $3d$ states. These data are in close agreement with our obtained Mn d electronic structure at $U = 2.0$ eV (Fig. 3). Other physical properties of the system at this value of U are also in good agreement with experiment (Table I), except the band gap, which still seems to be significantly lower than the measured value. This is because the reported experimental band gap (2.0 eV) is mainly measured between the occupied majority and unoccupied minority Mn d states,[17] which is in agreement with our obtained Mn d partial DOS at $U = 2$eV (Fig. 3). Therefore, we adopted $U = 2$ eV for our GGA + U study on α-MnSe nanowires.

In order to understand the mechanism of magnetism in α-MnSe, one should take into account that this system in the main [100], [010], and [001] crystallographic directions is composed of principal linear MnSe chains. A principal MnSe chain, depending on the parallel or antiparallel alignment of the successive Mn spin moments, may have FM or AFM states. In AF111 α-MnSe, all MnSe chains are in the AF state, while in the AF001 and FM α-MnSe, the principal MnSe chains are in the FM state. The stability of antiferromagnetism in the [111] direction of α-MnSe indicates that the principal MnSe chains prefer the AF state. It is attributed to Se mediated Mn-Mn superexchange interactions in the system.[19] For a better understanding of the principal MnSe chains and their role in the electronic and magnetic behavior of the α-MnSe structures, we have studied free MnSe chains in different magnetic states. The obtained cohesive energies and band gaps after full atomic and structural relaxation within GGA + U ($U = 2$eV) are presented in Table II. The band gaps of ideal (unrelaxed) structures are also given for comparison.

TABLE II. The cohesive energy E_C(mRy/atom) and band gap (eV) of α-MnSe free chains and free surfaces within different spin orders. The last two columns are the band gaps of relaxed and unrelaxed structures, respectively.

System	State	E_C	Gap	Gap*
Free chain	AF	−228.5	2.25	0.63
	FM	−197.1	0.03	none
Free (100) surface	AF111	−286.5	1.32	1.07
	AF001	−285.3	0.35	0.06
Free (110) surface	AF111	−280.6	0.85	0.61
	AF001	−279.5	0.17	0.07

As predicted, the AF state of the free chain is found to be considerably more stable than the FM state.

The electronic properties of MnSe chains are found to be strongly associated with their magnetic states. While in the AF state a rather large gap is calculated for this system, there is almost no gap in the FM state. This behavior is attributed to the bonding between the valence Mn $4s^2 3d^5$ and Se $4p^4$ shells. The ionic hybridization between the Se $4p^4$ and the Mn $4s^2$ states leaves three nearly filled Se $4p$ states pointing toward nearest-neighbor Mn atoms in the x, y, and z directions. Therefore, the Mn-Se bonding mainly occurs between nearly filled Se $4p$ and half-filled Mn $3d$ orbitals. Since each Se p orbital has two electrons of opposite spin, the effective Mn-Se bonding happens when the adjacent Mn atoms in the chain have antiparallel spin moment. Ferromagnetic alignment of the adjacent Mn atoms in the chain substantially weakens the bonding-antibonding splitting in the system and, consequently, give rises to a near-metallic electronic structure (Table II).

The smaller band gap of the ideal AF MnSe chain, compared with the bulk value, is due to the lower number of Mn-Se bonds in the chain. Since the free chain atoms, compared with the six coordinated bulk atoms, have four broken bonds, the bonding-antibonding splitting in the ideal chain is considerably reduced. However, we observe that structural relaxation strongly increases the band gap of the free chain to about 2.25 eV, which is much higher than the calculated bulk value (1.30 eV). This is evidence for effective rehybridization of the broken bonds and formation of strong Mn-Se bonds in the relaxed MnSe chain. It will be explained that this effective rehybridization passivates the MnSe nanostructures and preserves the semiconducting character of the system.

IV. MnSe[001] NANOWIRES

A. Morphology

According to the experimental data, the MnSe one-dimensional nanostructures have a single-crystalline rock-salt α-MnSe structure, grown typically in the [001] crystallographic direction.[10] It is consistent with the general argument of Allen that a nanocrystalline nanowire prefers to be grown around the symmetry axis of the system.[20] Therefore, in this work, we study α-MnSe nanowires (NWs) in the stoichiometric [001] direction. Among the various possible cross sections in this direction, we focus on the highest-symmetry ones, which are dipole free and constructed from the low index

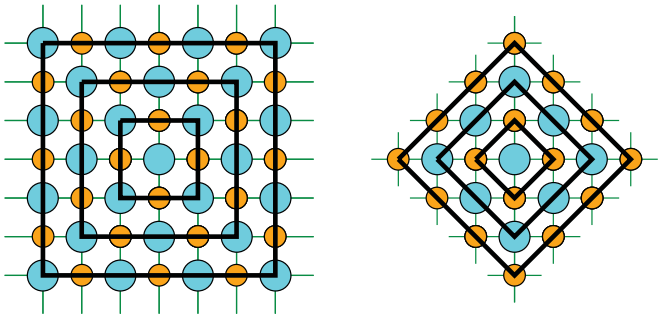

FIG. 4. (Color online) The first (smallest), second, and third (largest) sizes of square and lozenge nanowires studied in this paper. The larger (blue) and smaller (orange) circles stand for Mn and Se atoms, respectively.

(100) and (110) facets. These cross sections are sketched in Fig. 4. The nanowires with equivalent (100) and (010) facets are called square nanowires (SQNWs), while those with equivalent (110) and ($\bar{1}$10) facets are called lozenge nanowires (LZNWs). We have investigated the structural, electronic, and magnetic properties of the three smallest sizes of SQNWs and LZNWs, as shown in Fig. 4.

As shown in Fig. 4, the facet atoms in SQNWs and LZNWs have one and two broken bonds, respectively, while the edge atoms in each case have one more broken bond. Therefore, SQNWs are expected to be more stable. In order to verify this expectation, before direct NW calculations, we computed the free (100) and (110) surface energies of α-MnSe with AF001 and AF111 spin order. These free surfaces are simulated by slab supercells containing seven stoichiometric MnSe layers and a vacuum thickness of about 10 Å to prevent interaction between adjacent slabs. The in-plane lattice parameters of the free-surface slabs were set to the corresponding bulk values, while all atomic positions were fully relaxed. The cohesive energies and band gaps of the relaxed α-MnSe free surfaces are given in Table II, along with the band gaps of the unrelaxed structures for comparison. As predicted, the (100) free surface is found to be more stable, fortifying our expectation of more stability in SQNWs compared with LZNWs. In both surfaces the bulk-like AF111 spin ordering is more stable than AF001. It shows that surface effects do not change the superexchange mechanism and, consequently, AF spin ordering of the surface MnSe chains.

The band gaps of the ideal MnSe surfaces in the AF111 state are determined to be smaller than the bulk value. Similar to the free chain results, this is attributed to the lower coordination of the surface atoms in the system. The surface atoms in the free (100) and (110) surfaces have one and two broken bonds, respectively. The larger band gap of the free (100) surface compared with the (110) surface is clearly due to the lower number of broken bonds in this system. The enhancement of the free-surface band gaps, after structural relaxation, is more evidence for efficient rehybridization of the surface broken bonds in the α-MnSe nanostructures.

B. Physical properties

In order to address the structural stability of α-MnSe NWs, we calculated the three narrowest SQNWs and LZNWs. These simulations were done in tetragonal supercells containing a nanowire surrounded by a vacuum thickness of about 11 Å in the x-y plane to prevent interaction between adjacent wires. Although the stable spin ordering in the bulk as well as free (100) and (110) surfaces of α-MnSe is the type II antiferromagnetism (AF111), possible edge effects may stabilize different magnetic states in narrow MnSe nanowires. Therefore, all SQ and LZ nanowires were calculated in both AF111 and AF001 states. Moreover, in the cases of the first-size SQNW and LZNW, FM states were also considered and found to be about 14 and 9 mRy/atom less stable than the AF001 states, respectively. Hence, for larger NWs the ferromagnetic states were ignored in our investigation.

The computed properties of the first, second, and third sizes of SQNWs and LZNWs in the AF111 and AF001 magnetic states, after full relaxation of the atomic positions, are listed in Table III. In order to relax the possible surface-induced stresses, the vertical c lattice parameter of all studied NWs, except the third size SQNWs, was accurately optimized. Since the optimized c value of the second-size SQNW is rather close to bulk, in order to avoid huge computational demands, in the third-size SQNWs the bulk lattice parameters were adopted.

TABLE III. The physical properties of various α-MnSe[001] nanowires in AF111 and AF001 states. SQ-i, SQ-i*, and LZ-i indicate ith-size SQNWs, smoothed SQNWs, and LZNWs. Here nbb is the number of broken bonds per atom, bond (Å) indicates the average Mn-Se bond length in the NW, E_C(mRy/atom) is cohesive energy, Y (GPa) is Young's modulus, μ_{Mn} and μ_{Se} (μ_B) are the average magnetic moments of Mn and Se atoms, respectively, and gap and gap* (eV) are the energy band gap of NWs after and before structural relaxation, respectively.

		AF111								AF001							
Nanowire	nbb	c	Bond	E_C	Y	μ_{Mn}	μ_{As}	Gap	Gap*	c	Bond	E_C	Y	μ_{Mn}	μ_{As}	Gap	Gap*
SQ-1	1.5	9.70	2.66	−275.6	233	4.71	0.01	1.71	0.90	9.70	2.67	−274.8	253	4.80	0.04	1.07	none
SQ-2	1.25	10.02	2.70	−281.8	128	4.68	0.01	1.64	1.14	10.02	2.69	−280.5	144	4.89	0.02	0.95	none
SQ-2*	1.66	9.86	2.66	−278.9	135	4.68	0.01	1.36	0.86	···	···	···	···	···	···	···	···
SQ-3	1.16	10.35	2.74	−283.4	···	4.69	0.02	1.40	1.23	10.35	2.74	−282.3	–	4.84	0.04	0.33	none
SQ-3*	1.29	10.35	2.76	−282.4	···	4.70	0.02	1.11	1.04	···	···	···	···	···	···	···	···
LZ-1	3	8.97	2.57	−250.8	265	4.66	0.03	1.58	none	8.97	2.58	−248.7	287	4.80	0.05	0.84	none
LZ-2	2.5	9.28	2.62	−266.5	145	4.68	0.02	1.42	0.14	9.38	2.69	−266.2	160	4.77	0.03	0.60	none
LZ-3	2.33	9.60	2.74	−272.7	121	4.70	0.01	1.19	0.99	9.60	2.74	−272.6	138	4.79	0.03	0.14	none
Bulk	···	10.35	2.75	−289.2	110	4.66	0.0	1.30	···	10.35	2.76	−287.6	125	4.84	0.04	none	···

The resulting Young's modulus from the performed lattice optimizations are listed in Table III. The nanowire Young's modulus and equilibrium c values are observed to be larger and smaller than the bulk values, respectively, indicating enhancement of the Mn-Se bonds at the nanowire surfaces. This fact confirms efficient rehybridization of the surface broken bonds in the MnSe nanowires. As a result, the LZ-1 nanowire with the highest number of broken bonds per atom has the lowest c value and the highest Young's modulus in both the AF111 and AF001 magnetic states.

Comparing the energy band gaps of the ideal and relaxed NWs (especially in the narrower wires) indicates strong enhancement of these parameters after structural relaxation. This enhancement in the AF001 nanowires is so strong that, contrary to the corresponding bulk value, it opens a rather large gap in the system. This phenomenon is also attributed to the efficient rehybridization of the surface broken bonds after structural relaxation, which strengthens Mn-Se bonding at the nanowire surfaces. This important phenomenon is very visible in the behavior of the average Mn-Se bond length in the nanowires (Table III). The narrower the nanowire is, the lower the average bond length is, the stronger the Mn-Se bond is, and the higher the energy of the band gap is. From another point of view, one may argue that rehybridization of the surface broken bonds enhances quantum confinement of the surface electrons in the nanowire potential well and, consequently, increases the band gap. In all cases, by increasing the NW size, the energy band gaps and average bond lengths approach the corresponding bulk values. The calculated atomic magnetic moments in the nanowires are close to the corresponding bulk values, indicating weak surface exchange enhancement in the systems. This fact provides magnetic evidence for strong Mn-Se bonds at the nanowire facets and edges.

In order to discuss the stability of NWs, the cohesive energy E_C is calculated as follows:

$$E_C = \frac{E_{NW} - \left(N_{\mathrm{Mn}}\epsilon_{\mathrm{Mn}}^{\mathrm{atom}} + N_{\mathrm{Se}}\epsilon_{\mathrm{Se}}^{\mathrm{atom}}\right)}{N_{\mathrm{Mn}} + N_{\mathrm{Se}}}, \qquad (1)$$

where E_{NW} is the nanowire total energy, N_X is the number of X atoms in the nanowire, and $\epsilon_X^{\mathrm{atom}}$ is the total energy of an isolated X atom calculated in a large, single-atom, simple cubic supercell. The computed cohesive energies indicate that in all cases the AF111 magnetic state is more stable. It was already discussed that in the AF111 state, all principal MnSe chains have AF spin order and hence strong Mn-Se bonds form in the system. While in the AF001 states, the principal MnSe chains have FM spin order, wherein Mn-Se bonding is considerably weaker. Metallic (no gap) behavior of the unrelaxed AF001 nanowires confirms weaker Mn-Se bonding in the systems compared with AF111 nanowires.

In order to compare the stability of SQNWs and LZNWs, one should take into account the different sizes of these systems. Therefore, for accurate comparison, we define the effective radius of a nanowire as the radius of a circle with the same area as the unrelaxed nanowire cross section. The effective radii of nanowires are listed in Table IV, and the plot of cohesive energy as a function of radius is presented in Fig. 5. It is clearly visible that SQNWs are more stable than LZNWs. As argued before, it is attributed to the higher coordination of surface atoms and thus lower number of broken bonds in the SQNWs facets and edges. The edges and (100) facets of SQNWs have one broken bond per surface atom less than edges and (110) facets of LZNWs.

TABLE IV. Effective radius R, number of edge (N_{edg}), number of facet (N_{fac}), and total number (N_{tot}) of principal MnSe chains in the nth-size SQNWs and LZNWs.

	LZNW	SQNW
R (Å)	$2.20n$	$3.11n$
N_{edg}	4	4
N_{fac}	$4(n-1)$	$4(2n-1)$
N_{tot}	$2n(n+1)+1$	$4n(n+1)+1$

In order to see whether the stable SQNWs prefer sharp or smooth edges we constructed and calculated second- and third-size smoothed square α-MnSe nanowires by removing the edge MnSe chains in the second- and third-size SQNWs, respectively. Since the stable magnetic state of all studied MnSe systems in this work (including bulk, surface, and nanowire) was found to be type II antiferromagnetism (AF111), the smoothed SQNWs were only considered in the AF111 spin state. The obtained physical properties of the two studied smoothed SQNWs are given in Table III. Comparing the cohesive energies of the smoothed and normal SQNWs and free antiferromagnetic MnSe chains (Table II) indicates that removing edge MnSe chains in the second and third SQNWs requires energies of about 69 and 66 mRy/atom, respectively. Therefore, we conclude that the edge chains, in spite of their low coordinations, enhance stability of SQNWs, and as a result, narrow α-MnSe NWs prefer square cross sections with sharp edges.

C. Phenomenology of cohesive energies

It was argued that the principal MnSe chains play an important role in the magnetic and subsequently electronic properties of MnSe nanowires. For a better understanding of the surface effects on the principal MnSe chains, we employ a phenomenological model that expresses the cohesive energy

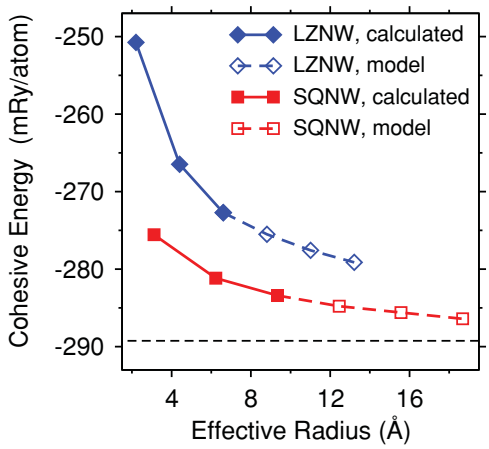

FIG. 5. (Color online) The calculated and extrapolated (model) cohesive energies of SQNWs and LZNWs as a function radius.

of nanowires E_C^{nw} as a function of facet and edge MnSe chain energies:[21]

$$E_C^{nw} = E_C^{bulk} + \frac{N_{fac}}{N_{tot}}\epsilon_{fac} + \frac{N_{edg}}{N_{tot}}\epsilon_{edg}, \quad (2)$$

where E_C^{bulk} is the bulk cohesive energy, N_{fac} and N_{edg} are the number of facet and edge chains, respectively, ϵ_{fac} and ϵ_{edg} are the facet and edge chain energies, respecitvely, and N_{tot} is the total number MnSe chains in the nanowire. The MnSe chain energies phenomenologically measure the energy cost to create principal MnSe chains at the nanowire facet and edges and are determined by fitting the model to the obtained cohesive energies of three narrowest SQNWs and LZNWs. Moreover, by extrapolating the model energy, one may estimate the cohesive energy of some larger NWs without direct calculation of these systems.

In order to fit the model to the calculated cohesive energies of NWs, one should take into account the size dependency of ϵ_{edg} and ϵ_{fac}, especially at small radii. These energy parameters are expected to decay by increasing R to converge to some constant values. Obviously, the converged values of ϵ_{fac} in large radii should coincide with the calculated free-surface results. In order to measure the energy costs for creation of MnSe chains at the (100) and (110) free surfaces, we applied Eq. (2) to the free-surfaces cohesive energies and found $\epsilon_{100} = 9.45$ and $\epsilon_{110} = 30.10$ mRy/atom. We propose the following simple and reasonable form of ϵ_{fac} and ϵ_{edg} as a function of nanowire radius R:

$$\epsilon_{fac} = a + \frac{b}{R^m}, \quad \epsilon_{edg} = c + \frac{d}{R^n} \quad (3)$$

After inserting the above chain energy functions into Eq. (2), the model was fitted to the calculated cohesive energies of the first-, second-, and third-radii SQNWs and LZNWs.[22] The best values of the fitted parameters for both SQNWs and LZNWs are presented in Table V, and the resulting chain energy plots are displayed in Fig. 6. As argued, the fitted values of a are close to the MnSe chain energies at free (100) and (110) surfaces. It is observed that both facet and chain energies decay by R^{-2}. In order to extrapolate the cohesive energy of some larger NWs by using Eq. (2), we determined the N_{fac}, N_{edg}, and N_{tot} parameters of forth- to sixth-size NWs by using the given formula in Table IV. The extrapolated data are depicted in Fig. 5. As expected, with increasing radius, the contributions of facet and edge chain energies decrease, and nanowire cohesive energy approaches the bulk value.

It is obviously seen (Fig. 6) that the LZNW edge and facet chain energies are much higher than SQNWs, indicating much higher energy costs for creation of the LZNWs surface chains. Therefore, the formation of narrow α-MnSe NWs with (100) facets is much more probable. Although at very large sizes the cohesive energy of LZNWs approach that of SQNWs, they do not cross any where in Fig. 5, indicating more stability of SQNWs in a broad range of radii.

TABLE V. The best-fit parameters of the chain energy models.

	a (mRy)	b (mRy Å^2)	m	c (mRy)	d (mRy Å^2)	n
SQNW	9.54	12.31	2	22.70	8.22	2
LZNW	30.56	63.30	2	57.55	47.63	2

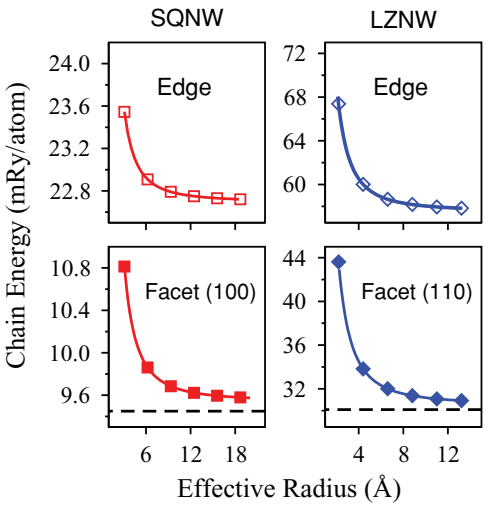

FIG. 6. (Color online) The edge and facet chain energies as a function of radii in (left) SQNWs and (right) LZNWs. The dashed lines indicate corresponding free surface chain energies.

V. PASSIVATION OF NANOWIRES

Passivation of surface dangling bonds is an important issue in theoretical studies of semiconductor nanostructures. In practice, these active dangling bonds are saturated via adsorption of various environment atoms and/or surface reconstruction. Without passivation, the surface dangling bonds may introduce localized electron states near the Fermi level, ruining the electronic and optical properties of the nanostructure and making it useless for most applications.[21,23] Well-defined energy band gaps are necessary to be able to consider the potential optical applications of NWs.

In order to examine the effect of surface dangling bonds on the properties of α-MnSe NWs, we calculated and studied the first-size SQNW passivated with pseudo hydrogen atoms. After full relaxation of the atomic positions and vertical lattice parameter, the electronic structure of passivated nanowire was calculated and compared to the corresponding pristine wire. The optimized c value of the passivated wire was found to be 10.95 bohr, significantly larger than the c value of the first-size pristine SQNW (9.70 bohr). This fact indicates that passivation by hydrogen atoms significantly weakens the surface bonds of MnSe nanowires. Assuming a source of H_2 molecules for passivation, the adsorption energy of hydrogen atoms to the first-size SQNW was determined to be about 19 mRy/atom. The positivity of the hydrogen adsorption energies is further evidence for weaker surface bonding in the passivated wires. The electronic band structures of the pristine and passivated first-size α-MnSe NWs are shown in Fig. 7. In both spin channels, it is clearly observed that passivation has a negligible effect in the energy band gaps.

These observations clearly contradict the physical expectation that saturation of the surface dangling bonds should enhance the energy band gap as well as the stability of the system. Therefore, we conclude that there are no surface dangling bonds at the surfaces of α-MnSe nanowires. In

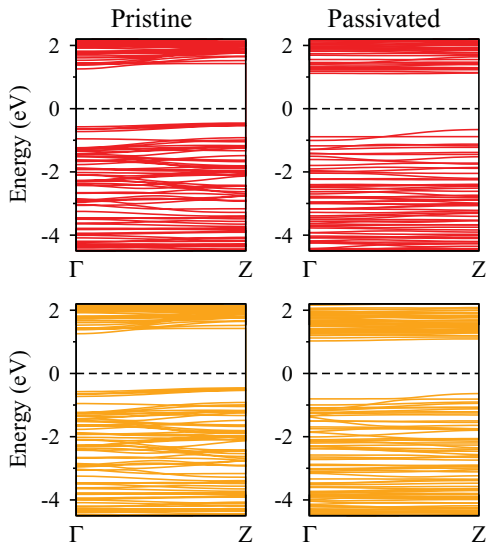

FIG. 7. (Color online) (top) The majority (red) and (bottom) minority (orange) energy band structure of the (left) pristine and (right) passivated first-size α-MnSe[001] square nanowire. The Fermi energies are set to zero.

other words, these systems, in contrast to most conventional semiconductor nanostructures, are self-passivated and need not to be passivated by hydrogen atoms. The mechanism of this self-passivation is the effective rehybridization of the surface broken bonds observed in the free chain, free surfaces, and pristine nanowires of α-MnSe. As argued before, the surface broken bonds in various MnSe nanostructures merge into the existing bonds and, consequently, enhance the semiconductor character of system.

VI. SUMMARY

In this paper we have investigated physical properties of bulk, free chain, free (100) and (110) surfaces, and square and lozenge cross section nanowires of α-MnSe by using density functional pseudopotential calculations. It was shown that the GGA + U scheme with an effective U= 2.0 eV is required to reproduce the experimental bulk spin exchange splitting and energy band gap. We argued that the magnetic and, consequently, electronic properties of MnSe structures are controlled by principal MnSe chains. The GGA + U results indicate that the occurrence of (100) facets in narrow α-MnSe nanowires is significantly more likely than (110) facets and these systems prefer square cross sections with sharp edges. Phenomenological energy costs for creation of facet and edge MnSe chains were calculated as a function of nanowire size and were found to converge to 9.5 and 22.7 mRy/atom, respectively, at large radii of the stable square nanowires. Because of the efficient rehybridization of the surface broken bonds, the MnSe nanostructures were found to be free of the surface dangling bonds and hence self-passivated.

ACKNOWLEDGMENTS

This work was supported jointly by the Vice Chancellor for Research Affairs of Isfahan University of Technology, Center of Excellence for Environmental nanotechnology, and ICTP Affiliated Centre. We thank our colleague Mojtaba Alaei for helpful discussions.

[1] S. A. Wolf, D. D. Awschalom, R. A. Buhrman, J. M. Daughton, S. Molnr, M. L. Roukes, A. Y. Chtchelkanova, and D. M. Treger, Science **294**, 1488 (2001).
[2] K. Ozawa, S. Anzai, and Y. Hamaguchi, Phys. Lett. **20**, 132 (1966).
[3] J. K. Furdyna, J. Appl. Phys. **64**, R29 (1988).
[4] D. R. Huffma and R. L. Wild, Phys. Rev. **118**, 526 (1966).
[5] R. J. Pollard, V. H. McCann, and J. B. Ward, J. Phys. C **16**, 345 (1983).
[6] P. Klosowski, T. M. Giebultowicz, J. J. Rhyne, N. Samarth, H. Luo, and J. Furdyna, J. Appl. Phys. **69**, 6109 (1991).
[7] L. Chen, H. Falk, P. J. Klar, W. Heimbrodt, F. Brieler, M. Froba, H. A. K. von Nidda, A. Loidl, Z. Chen, and Y. Oka, Phys. Status Solidi B **229**, 31 (2002).
[8] M. Wu, Y. Xiong, N. Jiang, M. Ning, and Q. Chen, J. Cryst. Growth **262**, 567 (2004).
[9] S. Lei, K. Tang, and H. Zheng, Mater. Lett. **60**, 1625 (2006).
[10] H. J. Chun, J. Y. Lee, D. S. Kim, S. W. Yoon, J. H. Kang, and J. Park, J. Phys. Chem. C **111**, 519 (2007).
[11] QUANTUM-ESPRESSO is a community project for high-quality quantum-simulation software, based on density functional theory and coordinated by P. Giannozzi. See [http://www.quantum-espresso.org] and [http://www.pwscf.org].
[12] For Mn and Se pseudopotentials, we used Mn.pbe-sp-van.UPF and Se.pbe-van.UPF, respectively, from the QUANTUM-ESPRESSO [http://www.quantum-espresso.org] distribution.
[13] J. P. Perdew, K. Burke, and M. Ernzerhof, Phys. Rev. Lett. **77**, 3865 (1996).
[14] H. J. Monkhorst and J. D. Pack, Phys. Rev. B **13**, 5188 (1976).
[15] M. Methfessel and A. T. Paxton, Phys. Rev. B **40**, 3616 (1989).
[16] D. L. Decker and R. Wild, Phys. Rev. B **4**, 3425 (1971).
[17] H. Sato, T. Mihara, A. Furuta, M. Tamura, K. Mimura, N. Happo, M. Taniguchi, and Y. Ueda, Phys. Rev. B **56**, 7222 (1997).
[18] The only magnetic measurement on α-MnSe is performed in a system doped with 0.05% Li and resulted in a Mn magnetic moment of 4.45 μ_B [S. J. Pickart *et al.*, Phys. Rev. **121**, 707 (1961)]. In order to estimate the value of the Mn moment in pure α-MnSe, we used the fact that the theoretical moment of Mn in the rock-salt and zincblende structures of MnSe is slightly larger than MnS [S. J. Youn *et al.*, Phys. Status Solidi B **241**, 1411 (2004); S. H. Wei and A. Zunger, Phys. Rev. B **48**, 6111 (1993)]. Since the experimental Mn magnetic moment in MnS is 4.54μ_B [B. E. F. Fender *et al.*, J. Chem. Phys. **48**, 990 (1968)], the corresponding value in MnSe was speculated to be about 4.6μ_B.

[19] A. Milutinovic, Z. V. Popovic, N. Tomic, and S. Devic, Mater. Sci. Forum **453-454**, 299 (2004).
[20] P. B. Allen, Nano Lett. **7**, 6 (2007).
[21] T. Sadowski and R. Ramprasad, Phys. Rev. B **76**, 235310 (2007).
[22] After several tries, we realized that the cohesive energies of lattice-optimized nanowires are not appropriate for our proposed phenomenology, probably because of the inconsistent lattice parameters on the two sides of Eq. (2). Hence, the cohesive energies of the relaxed nanowires with bulk lattice parameter were used for phenomenology.
[23] P. W. Leu, B. Shan, and K. Cho, Phys. Rev. B **73**, 195320 (2006).